Journal of Chromatography A, 1217 (2010) 6724–6732

Contents lists available at ScienceDirect

Journal of Chromatography A

journal homepage: www.elsevier.com/locate/chroma

Computer aided design optimisation of microfluidic flow distributors

Joris Vangelooven, Gert Desmet*

Vrije Universiteit Brussel, Department of Chemical Engineering (Transport Modelling & Analytical Separation Science Group), 1040 Brussels, Belgium

ARTICLE INFO

Article history:
Available online 1 June 2010

Keywords:
Microfluidics
Hydrodynamics
Miniaturisation
CFD

ABSTRACT

This study reports on a quantitative study of the influence of the most important geometrical design parameters for micro-machined flow distributors with uniform cross-section and filled with diamond-shaped pillars having their longest dimension oriented perpendicular to the axial flow direction. It was found that the shape of the bands eluting from the distributor improves with increasing aspect ratio (AR) of the pillars, both in terms of global warp and local axial dispersion. Increasing the AR from 5 to 25 reduces the distributor length needed to bring the maximal transversal velocity difference below 5% from 170 μm to 15 μm when using pillars with axial width of 5 μm. To solve the problem that high AR pillar distributors only have a limited number of exit points, and therefore produce bands with a strong local warp, one can conceive mixed size distributors, wherein a zone filled with several rows of very high AR pillars is followed by one or more zones consisting of pillars with a smaller AR. With such a design, the variance of the eluting bands can be reduced to only 30% of the variance of a single size distributor.

1. Introduction

Hyphenating high efficiency chromatographic separation columns to pre- and post-column processes without losing too much of the efficiency potential of the column becomes especially difficult when miniaturised systems such as those encountered in lab-on-a-chip applications or those needed to do proteomics or single cell analysis need to be used. In the past, many miniaturized and lab-on-a-chip systems have been proposed wherein the separation column has a flat-rectangular cross-section to increase its loadability [1–5]. In this case, the connection problem becomes especially difficult because the flow and the sample entering the column via a narrow feed channel need to be distributed evenly across the whole cross-section of the column, which can be several millimetres wide. The same problem occurs at the column exit, where the mobile phase and the sample components need to be recollected into a narrow exit channel before being transported to the detector or another post-column process.

Previous work considering the design of microfluidic flow distributors has, amongst others, been performed by Giddings et al. [6,7] and Sant et al. [8]. The present study builds further upon a previous (experimental) study [9] wherein we compared the performance of a number of different flow distributor designs that can be used to connect flat-rectangular chip-based channels to circular or square connection channels. In Ref. [9], it was observed that distributors filled with distributor elements (or pillars) with a high aspect ratio (AR) are needed and that radially interconnected distributors are to be preferred over bifurcating distributors. This AR is defined as in Ref. [9]:

$$\mathrm{AR} = \frac{w_\mathrm{p}}{\ell_\mathrm{p}} \tag{1}$$

with w_p and ℓ_p respectively the width and length of the pillars.

Given the large freedom of design offered by the microfabrication methods that are used to fabricate lab-on-a-chip devices, the designs considered in Ref. [9] however only represent a very small segment of all technically possible distributor designs, so that a more comprehensive study was needed to arrive at a truly optimised microfluidic flow distributor design. To gain a fundamental understanding of the different parameters affecting the distributor performance and to scan through a large number of designs in a short time, the present study relied on the use of computational fluid dynamics (CFD) simulations to calculate the flow field and species dispersion pattern in a large variety of different distributor designs. The use of numerical simulations to design microfluidic components such as bends, distributors, injection crosses etc. is well adopted in the field and has been used in many literature references [10–15].

To limit the scope, only flow distributors with a uniform cross-section (divergence angle $\alpha = 180^\circ$, see Fig. 1) are considered, although it is well known [8,7,9,16] that better results can be obtained with distributors with a diverging cross-section (ideally $\alpha < 180^\circ$). For Field Flow Fractionation (FFF), channels with an optimal divergence angle of $60^\circ < \alpha < 90^\circ$ have already been proposed [7]. The design problem in the uniform cross-section case is however already rich enough to warrant a separate study, especially

* Corresponding author. Tel.: +32 26293251; fax: +32 26293248.
E-mail address: gedesmet@vub.ac.be (G. Desmet).

0021-9673/$ – see front matter © 2010 Elsevier B.V. All rights reserved.
doi:10.1016/j.chroma.2010.05.032

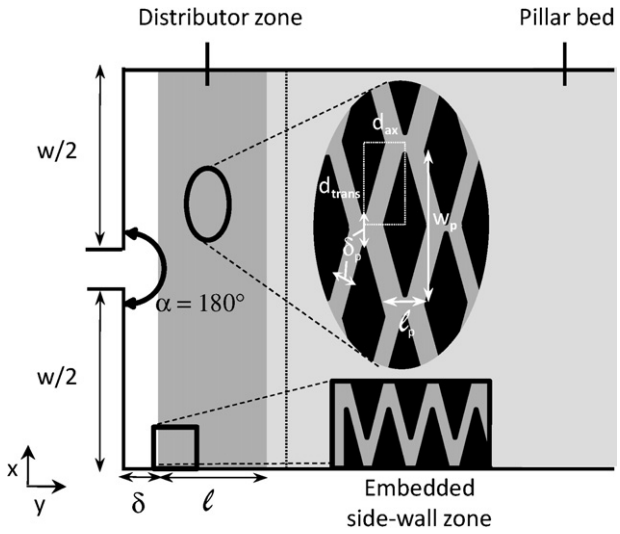

Fig. 1. (a) Geometrical definitions of important parameters in distributor design: w: column width, δ: gap width before distributor, ℓ: distributor length, d_{trans}: transversal domain size of distributor pillar grid, d_{ax}: axial domain size of distributor pillar grid, ℓ_p: axial pillar length, w_p: transversal pillar width, δ_p: minimal inter pillar distance.

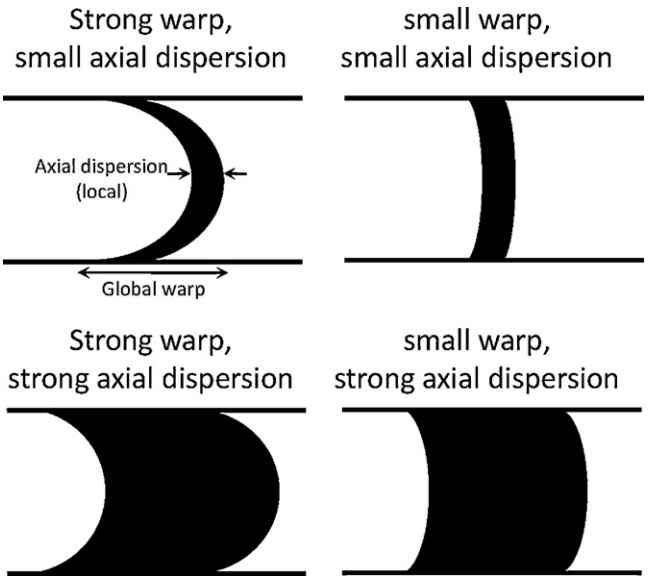

Fig. 2. (a–d) Different combinations of low and high local axial dispersion on the one hand and small and large overall band warp on the other hand.

considering that the optimisation of the uniform cross-section case is anyhow needed as a first step in the design of the diverging cross-section.

Another motivation for the consideration of distributors with a uniform cross-section is that we also wanted to gain insight in the flow distribution that occurs in real columns, where distributor frits are used that also have a uniform cross-section.

As a general rule, it can be said that a good flow distributor needs to spread out the flow maximally in the radial (denoted here further as "transversal") direction, which is automatically ascertained when the ratio of transversal to axial bed permeability (K_{trans}/K_{ax}) is maximized [17,18]. In some literature, this ratio is defined as the distributor or frit quality (FQ = K_{trans}/K_{ax}) [10,19]. Obviously, a high FQ can be obtained by filling the distributors with pillars that have a high AR and have their largest dimension oriented perpendicular to the axial flow direction. However, it is not known how high this AR can be made before the extra tortuosity and flow-through path obstruction it induces leads to an undesirably high axial dispersion or flow resistance. Finding out whether or not an optimal AR exists was therefore one of the main research questions at the origin of the present study.

Before proceeding, it is also important to distinguish between the two main types of band broadening that can be observed at the exit of a flow distributor. Both types are schematically represented in Fig. 2. The first type will be denoted using the term "global band warp". This global warp is essentially caused by the lateral differences in axial velocity at the outlet plane of the distributor. Note that in the absence of a flow distributor the band warp would be maximal, and a good distributor therefore helps to counter the warp.

The second type of band broadening is the local axial dispersion, caused by the dispersion phenomena occurring inside the individual through pores of the distributor. As indicated in Fig. 2a, this type of band broadening especially influences the local width of the bands eluting from the distributor, whereas the warp relates to their overall shape. Obviously, the best distributor is the one that combines both a small warp and a small local axial dispersion (Fig. 2d).

In the first part of the study, only distributors composed of uniformly sized pillars are considered. In the second part, mixed pillar size distributors are considered. Although all presented results pertain to the inlet distributor, it should be kept in mind that a fully similar flow distribution problem occurs at the exit of the separation bed.

2. Numerical procedures and considered geometries

With reference to Fig. 1, the different geometrical design parameters that have been considered in the present study were: the gap width (δ) before the actual distributor zone, the axial length of the distributor (ℓ) and the aspect ratio of the elongated pillars (AR). Only diamond-shaped pillars have been considered because this is the shape that fills up the space in the most uniform way and previous simulation work has shown that beds of uniformly packed diamond-shaped pillars lead to a very uniform local velocity distribution [20]. Because the smallest dimension in the system is the distance δ_p between two adjacent pillars, this distance was considered as a given design constraint, and was chosen equal to the minimal feature size that can be resolved with a 100% certainty during the etching process (here taken equal to $\delta_p = 2.5\,\mu m$). The positions of the pillar centres were calculated such that both the transversal distance between two diamond tips and the distance between two diamonds, perpendicular to the sides, were equal to δ_p. These two constraints lead to the following expressions for the axial and transversal domain sizes, depicted in Fig. 1:

$$d_{trans} = w_p + \frac{\delta_p}{2} \quad (2)$$

$$d_{ax} = [\delta_p \cos(AR) + (AR\,\delta_p \sin(AR))] - \left[AR\left(\frac{\ell_p}{2}AR + \frac{\delta_p}{2}\right)\right] + \frac{\ell_p}{2} \quad (3)$$

As a consequence of this design algorithm, the external porosity ε of the distributor beds remained nearly constant. Table 1 shows that ε only varies from 0.526 (AR = 5) to 0.505 (AR = 25). For the AR = 1-case, the ε-value is significantly larger ($\varepsilon = 0.652$), but this case is anyhow unfavourable (see results and discussion) and is not further considered. Since the ε-value of the useful AR-shapes lies close to that of a packed bed (for which typically $\varepsilon = 0.4$), this also implies that the mean axial velocity u_{mean} in the through pores of the distributor will be similar to that in the through pores of the

Table 1
Properties for the different distributor geometries: porosity ε, axial and transversal permeabilities (K_{ax}, K_{trans}), frit quality FQ (K_{trans}/K_{ax}) and the Van deemter constants from Eq. (9).

AR	ε	K_{ax} (10^{-13} m^2)	K_{trans} (10^{-13} m^2)	FQ	A	B	C
1	0.652	3.985	3.599	0.903	0.0502	1.4288	0.0042
5	0.526	0.522	5.431	10.397	0.0207	0.2185	0.0075
10	0.513	0.164	5.411	33.058	0.0077	0.0638	0.0089
15	0.508	0.079	5.370	67.864	0.0050	0.0291	0.0089
20	0.506	0.047	5.343	114.527	0.0031	0.0178	0.0090
25	0.505	0.031	5.324	172.701	0.0014	0.0118	0.0093

separation bed. This mean velocity is given by:

$$u_{mean} = \frac{F}{A\varepsilon} \tag{4}$$

wherein F is the volumetric flow rate, A is the cross-section of the open bed or distributor (i.e., without pillars) and equal to the product of the bed or distributor width w and the bed or distributor depth, and ε is the bed porosity.

All simulated flow domains were generated using Gambit® v2.4.6 software. The same software was used to generate the discretization grids needed for the numerical solution of the species and impulse conservation equations. The flow domains with the discretized simulation grids were subsequently fed to a commercial computational fluid dynamics solver (Fluent® v6.1.22) to solve the conservation equations and calculate the velocity fields according to second order discretization schemes for the momentum and mass balances and a SIMPLEC discretization for the pressure-velocity coupling. All inlet velocities and pressures have been chosen such that a practically relevant u_{mean} (0.1–10 mm/s, $Re = 2.43 \times 10^{-4}$–2.43×10^{-2} for $\delta_p = 2.5$ μm and water as mobile phase) was obtained (examples: see Fig. 10).

Both microscopic and distributed geometrical models have been considered. In the first case, the flow field and species dispersion are calculated down to the microscopic level of the individual through pores. In the second case, the information of the microscopic simulations (axial and radial permeability) is used to calculate the species dispersion in a medium with uniform composition (i.e., without resolving the individual pillars). The typical size of the flow domains considered in the macroscopic level simulations was 10 by 0.5 mm, divided in 500 000–750 000 grid cells. For the microscopic level simulations, typical flow domain sizes were of the order of 50 μm–1 mm, divided in 100 000–300 000 grid cells. It was ensured that the obtained data were independent of the grid size as well as from the employed time step size, by reducing both values until the influence upon the obtained result dropped below 0.5%. All simulations were conducted in 2D.

When calculating the velocity fields in the microscopic flow domains, the pressure gradient was calculated as well. This allowed calculating the effective bed permeability using Darcy's law:

$$\frac{\Delta P}{L} = \frac{\mu u}{K_v} \tag{5}$$

wherein ΔP is the pressure drop over length L, μ is the dynamic viscosity of the liquid, u is the interstitial velocity of the liquid and K_v the effective bed permeability. By changing the orientation of the flow domain, both the axial and the transversal permeability could be calculated (obtained values are given in Table 1).

The breakthrough of the bands eluting from the distributor was recorded at some specific monitor lines (example: see dashed line in Fig. 1). Pulse response profiles such as those for example shown in Fig. 11 were obtained by integrating the species concentration of the passing bands over the full width of the monitor line. The molecular diffusion coefficient (D_{mol}) in all species simulations was set to be 10^{-9} m^2/s. Other fluid parameters were set equal to those of water, unless stated otherwise.

To quantify peak width, the spatial variance σ^2 of the intensity profiles has been calculated using the zeroth, first and second moment (M_0, M_1 and M_2). The expression used for the nth-order moment [21,22] is:

$$M_n = \int_0^\infty c(x)x^n \, dx \tag{6}$$

in which M_n is the nth moment of function $c(x)$, in this case, the intensity profile. According to this definition, the zeroth moment equals the integrated surface below the curve. The total peak variance can then be calculated according to the following expression:

$$\sigma^2 = \frac{M_2}{M_0} - \left(\frac{M_1}{M_0}\right)^2 \tag{7}$$

3. Results and discussion

3.1. Effect of δ

Knowing that a good flow distributor requires a high ratio of the transversal over the axial permeability, it seemed advantageous to provide a small open region (with width δ, see Fig. 1) just before the actual distributor bed. Without this region ($\delta = 0$ in Fig. 1), the pillars would have to be merged directly with the front wall of the separation bed and the corners of the distributor would be poorly permeated. By providing an open zone without any pillars, the fluid entering the bed is immediately offered a transversally oriented flow path with a minimal flow resistance, thus strongly contributing a high FQ. Enhancing transversal flow by leaving a highly permeable zone before the frit has also been suggested for HPLC-column headers [11]. The axial width of this zone however needs to be carefully optimised, as can be noted from Fig. 3a, showing how strongly the shape of the species bands leaving the flow distributor is affected by a small change in δ (note that δ is much smaller than the actual distributor length ℓ). As can be noted, the $\delta = 5$ μm case (mid panel of Fig. 3a) leads to the best peak shape (best combination of global warp and local axial dispersion). This is further quantified in Fig. 3b, showing how the spatial variance σ^2 of the species band varies with δ. Since the represented σ^2-values have been obtained by integrating the species bands over the full width of the separation bed, they contain the effect of both the local axial dispersion as well as of the global band warp.

Fig. 3b clearly shows that the minimal σ^2-value is obtained for a gap width of $\delta = 5$ μm. The existence of this optimum can be understood as follows: when δ is too small, the transversal flow resistance of the gap becomes too large with respect to the axial flow resistance of the actual flow distributor region. As a consequence, only a small fraction of the entering liquid is directly diverted in the transversal flow direction and the global band warp is increased. When δ is too large, a considerable axial dispersion is generated because of the broad parabolic flow profile that is established in the open pre-distributor zone. In addition, when this zone becomes too wide, part of it will be poorly permeated and will therefore act as a dead zone. For the presently considered geometry, the optimal axial width of the open pre-distributor zone was about

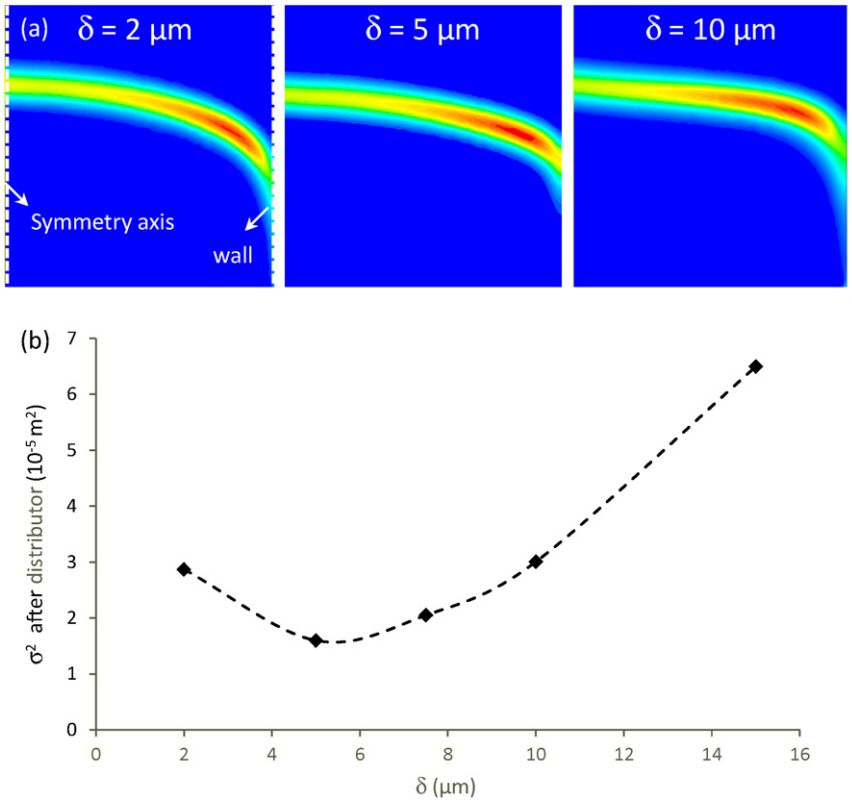

Fig. 3. (a) Top view of species bands eluting from distributors with different pre-distributor zone widths (δ = 2. 5 and 10 µm). Due to the axial symmetry, only half the column needs to be simulated with a symmetry boundary layer modelling the centre of the column. (b) Variation of the corresponding spatial band variance with δ. The 100 µm long distributor zone was defined to have the FQ of an AR 25 distributor, with the corresponding values for K_{ax} and K_{trans} (Table 1), u_{mean} = 2.5 mm/s. All simulations carried out with fluid parameters of water.

5 µm, i.e., about twice the width of the through pores in the actual distributor.

The importance of the gap width δ can be extrapolated to distributors with a diverging side wall ($\alpha < 180°$). In this case δ can be defined as the distance between the side wall and the first diagonal row of distributor pillars parallel to the side wall. If $\delta > \delta_p$ (the inter pillar distance), radial transport is facilitated by this low resistance transversal path towards the side wall, compensating for the inescapable difference in path length between the central zone of the column and the side wall zone. If δ is too large, an inverse situation will be created, in which the sample in the side wall zone runs ahead of the sample in the central region, leading to an inverse warp. The value of the ideal $\delta_{diverging}$ needs to be studied experimentally. Studying this parameter properly in a CFD study would call for a macro-size model with resolved distributor pillars including species transport. As this demands an extremely fine grid and an unsteady solver method, incorporating this search in a follow-up experimental study would be much more convenient.

3.2. Effect of ℓ_p and δ_p

Obviously, the axial extent of the pillars ℓ_p should be taken as small as possible, as there is no conceivable advantage that can be related to the use of pillars with a large ℓ_p-value. And also, at least from the perspective of reducing the local axial dispersion, the distance δ_p between the pillars should be kept as small as possible. Small δ_p-values have the drawback of leading to a poor bed permeability, but, as will be shown further on, the bed permeability is not a limiting factor in the design of microfluidic distributors for chromatographic separation columns.

In reality, the values of ℓ_p and δ_p are limited by the fabrication constraints, and more precisely by the minimal feature size that needs to be respected for the photolithography and the etching steps. Pillars that are smaller than this size are no longer resolvable during the etching step.

3.3. Effect of pillar aspect ratio (AR)

With ℓ_p and δ_p fixed by the fabrication constraints, the only optimisable parameter is the transversal width w_p of the pillars. To generalize the optimisation of this value, it is preferred to fix its value by a dimensionless number, the so-called aspect ratio (AR), defined in Eq. (1).

As already became apparent during our previous experimental study, the AR has a large influence on the distributor performance. Typical distributor performance measures are the transversal dispersion (D_{trans}) and the so-called frit quality number (FQ). Whereas the FQ-number can be calculated directly from the calculated axial and transversal bed permabilities (see Table 1), the transversal dispersion coefficient (D_{trans}) needs to be determined via a species dispersion simulation, based upon a numerical experiment wherein a continuous flow of dye enters the bed. As shown in Fig. 4a, this leads to a steady-state dispersion profile. Determining the transversal variance σ_{trans}^2 at different subsequent monitor lines, and plotting these values as a function of the mean breakthrough time, D_{trans} can be obtained from the slope of the expected straight line relationship, using:

$$\sigma_{trans}^2 = 2D_{trans}t \quad (8)$$

As can be noted from the D_{trans}-values represented in Fig. 4b and from the FQ-values given in Table 1, both measures strongly increase with increasing AR. This parallelism is in agreement with one's physical expectations, since the FQ-number can be considered

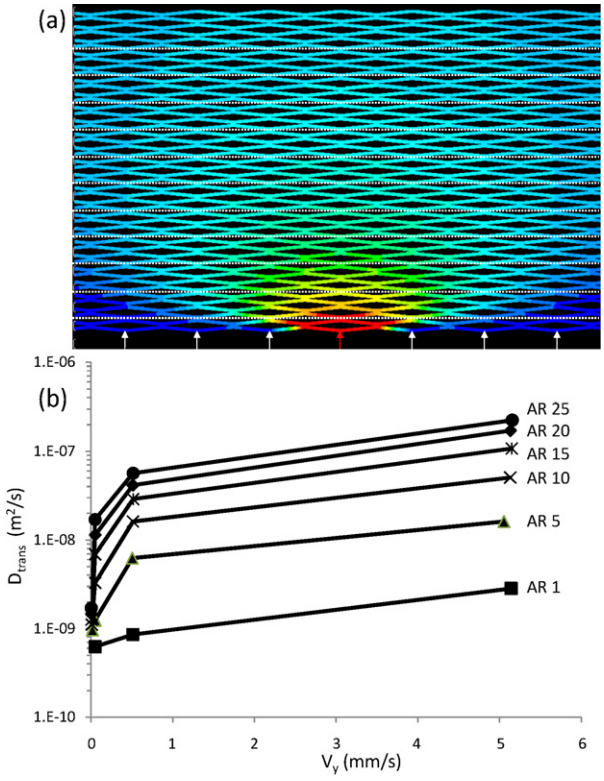

Fig. 4. (a) Top view of continuous injection simulations conducted to determine D_{trans}. The red arrow in the middle indicates the sample inlet, all other inlets (white arrows) are fed with water (blue). White dashed lines depict the monitor lines employed to calculate D_{trans} (Eq. (8)). (b) Evolution of transversal dispersion coefficient with aspect ratio and mean fluid velocity (Eq. (4)) with $D_{mol} = 10^{-9}$ and all other fluid properties of water.

as the causal parameter determining the D_{trans}-value. The lateral dispersion of the species in the distributor is namely essentially dominated by convection, i.e., by the velocity field, and the FQ-number expresses the ratio of the flow that is diverted transversally over that moving in the axial direction. The dominance of the convective process in the transversal dispersion can also be assessed from its actual value. As can be noted from Fig. 4b, this value is, depending on the fluid velocity, of the order of 10^{-8}–10^{-7} m^2/s. This is a factor of 10–100 larger than the molecular diffusion coefficient, and this high value can hence only be explained by the dominance of the convective transport.

3.3.1. Effect of AR on band warp

Since the transversal transport strongly increases with increasing AR of the pillars, it is also straightforward to expect that the velocity profile of the fluid leaving the distributor will become progressively more uniform with increasing AR. This can be readily assessed from the variation of the local velocity u in the transversal direction plotted in Fig. 5 (u represents the average fluid velocity in the individual through pores, i.e., averaged over the parabolic flow profile that is established in these pores).

Since the variation of the u/u_{centre}-parameter with y directly determines the global warp of the species bands leaving the distributor, the trends observed in Fig. 5 clearly imply that, the larger the AR of the pillars, the less the bands will be warped.

Repeating the velocity field calculation for different values of the mean velocity, it was observed that the plot shown in Fig. 5 is independent of the imposed velocity, so that the u/u_{centre}-profiles shown in Fig. 5 can be considered to be a unique feature of each considered AR. This finding is in agreement with the laminar nature of the flow, for it is a well-established fact that under laminar flow

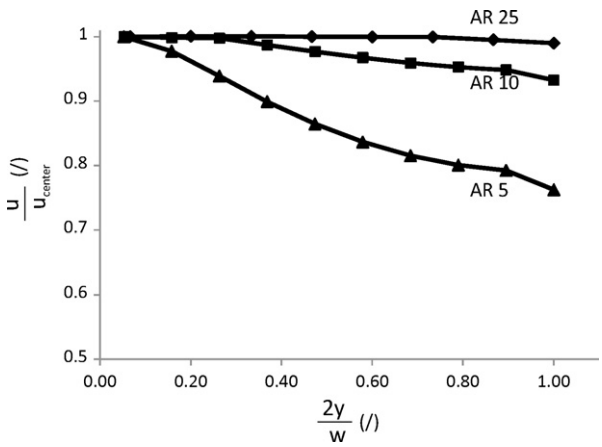

Fig. 5. The evolution of u/u_{centre} with varying AR. This parameter is a direct measure for the global warp of the species band leaving the distributor. ($\ell_p = 5$ μm, $\delta_p = 2.5$ μm, inlet velocity = 0.25 m/s).

conditions the relative velocity distribution is independent of the mean velocity.

3.3.2. Effect of AR on local axial dispersion

Fig. 6 shows the results of a series of axial dispersion calculations conducted inside the different considered distributor beds. The results are plotted as a reduced plate height ($h = H/\delta_p$) versus a reduced velocity ($\nu = (u\delta_p)/D_{mol}$, with $D_{mol} = 10^{-9}$). The h-values were obtained by mathematically imposing a rectangular pulse of tracer at the inlet plane of the distributor and by recording the breakthrough pulse at different monitor lines regularly spaced along the x-axis.

Not surprisingly, when considering that a distributor bed is nothing else but a packed bed system, the obtained h-curves display the same characteristic picture as obtained for the band broadening in any other packed bed system (B-term and C-term region embracing a curve minimum). Interestingly, the curve minimum decreases strongly with increasing AR. This is however in full agreement with the fact that any increase in AR of the transversally oriented diamond pillars leads to an additional hindering of the longitudinal diffusion (B-term band broadening). Most distributors will however be operated in the C-term region. Here it is interesting to note that the band broadening in this region is nearly perfectly linear and that the slope of the curve only increases slowly with increasing AR.

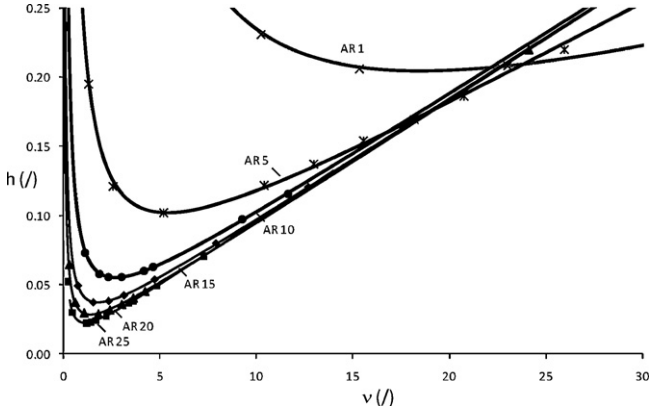

Fig. 6. Axial dispersion induced by the pillar arrangement inside the distributor for various degree of the AR and plotted as a reduced plate height ($h = H/\delta_p$) versus a reduced velocity ($\nu = u_{mean}\delta_p/D_{mol}$), with $\ell_p = 5$ μm, $\delta_p = 2.5$ μm, and $D_{mol} = 10^{-9}$ m^2/s.

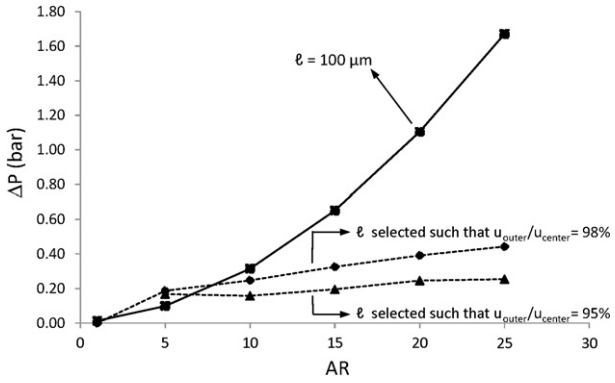

Fig. 7. Evolution of pressure drop with AR. Solid line depicts pressure drop for 100 μm long distributors. Dashed lines represent pressure drops for each of the distributors to obtain a u_{outer}/u_{centre} ratio of respectively 98% (upper) or 95% (lower curve) (ℓ_p = 5 μm, δ_p = 2.5 μm, u_{mean} = 5 mm/s).

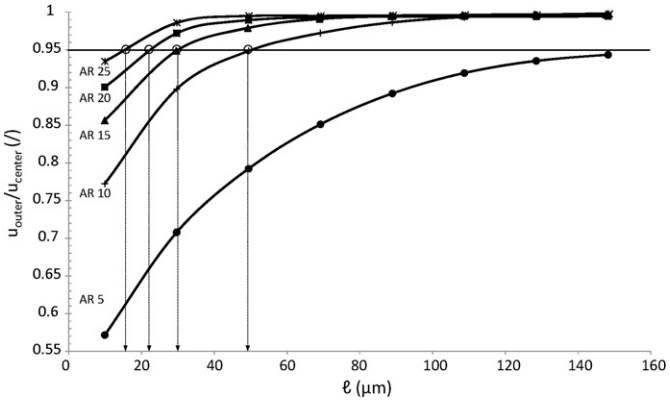

Fig. 8. Evolution of u_{outer}/u_{centre} with distributor length ℓ for five different values of the AR: AR 5 (lower)–AR 25 (upper). The vertical lines indicate the distributor length that would result in a maximal velocity difference of 5% between u_{outer} and u_{centre} (inlet velocity = 0.25 m/s, column width w = 1 mm, inlet width = 10 μm, δ = 5 μm, δ_p = 2.5 μm, ℓ_p = 5 μm).

Fitting the obtained data with the simple van Deemter model:

$$h = A + \frac{B}{\upsilon} + C\upsilon \quad (9)$$

A-, *B*- and *C*-term constants were obtained for the different distributor geometries. Their values are listed in Table 1, showing the sharp decrease of *B* with AR and a near constant *C*-term constant in the AR > 10-range.

3.3.3. Effect of AR on pressure drop

A clear drawback of transversally oriented pillars with a high AR is the fact that they generate a higher flow resistance than pillars with a smaller AR. However, considering that a good distributor maximally needs an axial length of 100 μm, while a typical separation bed is at least 5 cm longer, the pressure drop generated by a high AR flow distributor will generally be very small compared to the overall pressure drop of the bed, at least when considering chromatographic separation applications.

Fig. 7 shows how the pressure drop over a 100 μm long distributor and subjected to a flow rate of about 2.3 μL/min (mean linear velocity = 5 mm/s) varies with the AR. Obviously, the pressure drop increases strongly with the AR, but the resulting values are still relatively small due to the short distributor lengths that are needed. Even for the AR 25-case, the pressure drop is only about 14% of that across a 10 cm long separation bed filled with cylindrical pillars (value based on permeability simulations of cylindrical pillars with d_p = 5 μm) with flow resistance $K_v = 4.31 \times 10^{-13}$,), assuming that the distance between the pillars in the distributor is the same as the distance between the pillars making up the actual separation bed.

It should however be remarked that the sharp drop in permeability for increasing AR needs to be moderated by noting that the required distributor length decreases with increasing AR (see section 3.4), Fig. 7 also shows curves for the pressure drop over distributors delivering maximum velocity difference of respectively 2% or 5%. This is to compensate for the fact that the AR 25 distributor length for example only needs 10% of the AR 5 distributor length for the 5% velocity difference case. This 15 μm long AR 25 distributor then only delivers 2% of the total pressure drop over the 10 cm separation channel mentioned above.

3.4. Effect of distributor length

Using u_{outer}/u_{centre} (difference between *u*-value at $y = 0$ and $y = w/2$) as a characteristic measure for the uniformity of the velocity profile leaving the distributor outlet, Fig. 8 shows how the velocity profile progressively flattens when the distributor length ℓ increased. As expected, a high AR pillar distributor needs a shorter length to achieve a given degree of velocity uniformity. The dashed vertical lines indicate the ℓ needed for the different ARs to obtain a v_{outer} which is 95% of v_{centre}. As can be noted, ℓ can be brought back to less than 10% of its value by increasing AR from 5 to 25. The steepest drop in ℓ takes place from AR 5 to AR 10, but the further decrease for higher elongations is far from negligible, with still a 50% decrease from AR 15 to AR 25. This information was incorporated in Fig. 7 to calculate the pressure drop for different distributors to obtain this 95% velocity ratio.

Considering that the local axial dispersion is determined by the product of plate height H and bed length ℓ, and combining the strong reduction of the required distributor length with the fact that H nearly does not increase with the AR (cf. Fig. 6), it can be inferred that maximizing the AR of the pillars also leads to a minimization of the axial dispersion. This was unexpected, as we assumed at the beginning of the study that a high AR would automatically lead to a high local axial dispersion, because of the increased tortuosity of the flow-through pores. It now turns out that this effect is countered by the higher degree of transversal dispersion accompanying the increase in AR.

3.5. Effect of distributor exit points

Whereas the considerations made in Sections 3.3 and 3.4 all favour the use of high AR pillars, a major drawback of high AR pillars has been left unmentioned, which is that they lead to a reduction of the number of distributor exit points. Since the flow can only leave the distributor through the openings between the pillars, and since the lateral distance between these openings is equal to $w_p + \delta_p$ (see Fig. 1), it follows directly that a flow distributor filled with high AR pillars will only feed the separation bed at a limited number of locations (further on referred to as "exit points"). As a consequence, a new flow redistribution problem is created near each of these exit points, and the established flow profile consists of a series of warped shapes with period $w_p + \delta_p$. The exit point problem is illustrated in Fig. 9, showing the results of macro-scale simulations, in which the velocity at the different exit points are calculated using the microscale simulations leading to Fig. 5. It can clearly be observed from Fig. 9 that, considering the exit-point problem, there is a strong trade-off between global warp and local axial dispersion. For the low AR cases, the high number of exit points leads to a very low axial dispersion locally, but introduces a huge global warp due to a bad flow distribution

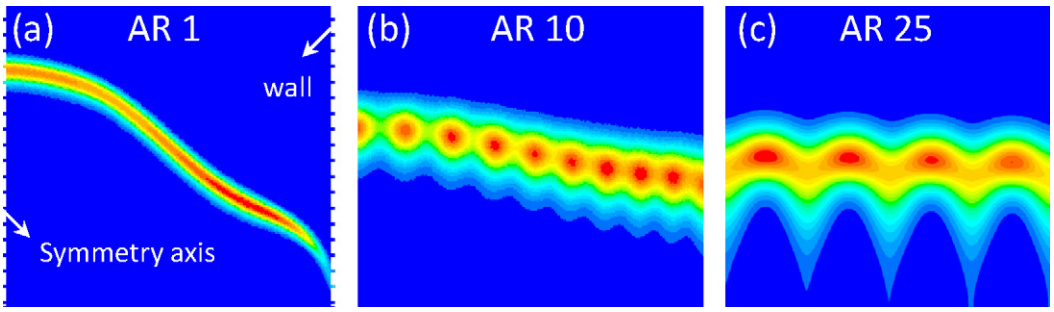

Fig. 9. Top view of species bands eluting from distributors with $\ell = 50\ \mu m$, different ARs, and as a consequence, also with a different number exit points: (a) AR = 2; (b) AR = 10; (c) AR = 25. Due to the axial symmetry, only one half the column needs to be simulated with a symmetry boundary layer modelling the centre of the column (column width $w = 1$ mm, $L_{col} = 5$ mm, $u_{mean} = 2.5$ mm/s, $D_{mol} = 10^{-9}$ m^2/s).

and the resulting inhomogeneous flow field (Fig. 9a). On the other hand, a (globally) straight band results from the highest AR case (Fig. 9c), but here the large distance between the (few) exit points leads to strong local warps. The importance of this exit-point problem can readily be understood by noting that there is an upper limit for the AR that can be applied in a bed with width w. This upper limit corresponds to the case wherein only one exit-point remains (this case arises when the AR is so high that $w_p = w$). In this case, the distributor no longer has any effect as the flow redistribution that needs to be done after the distributor is the same as in the case wherein there would have been no distributor at all.

At the outlet distributor, a similar problem occurs. Now because of the limited number of entry points, but the induced band broadening is fully identical.

3.6. Mixed size flow distributors

The obvious solution to resolve the problem of the limited number of exit-points discussed in Section 3.5 is to have a bed with sufficiently high AR elements followed by some convergence zone wherein the AR of the pillars is gradually decreased again, until the number of exit points approaches the number of parallel through pores in the actual separation bed.

To investigate the advantage of this approach, we compared a conventional single size flow distributor (with pure AR = 25 pillars, Fig. 10a) with three different mixed size flow distributors (all three going from AR = 25 to AR = 2.33, see Fig. 10b–d). The ARs of the second (and third) convergence zone were chosen such that their d_{ax}s (Eq. (3)) are compatible to that of the first zone. The performance of these different transitions to the pillar bed was examined by releas-

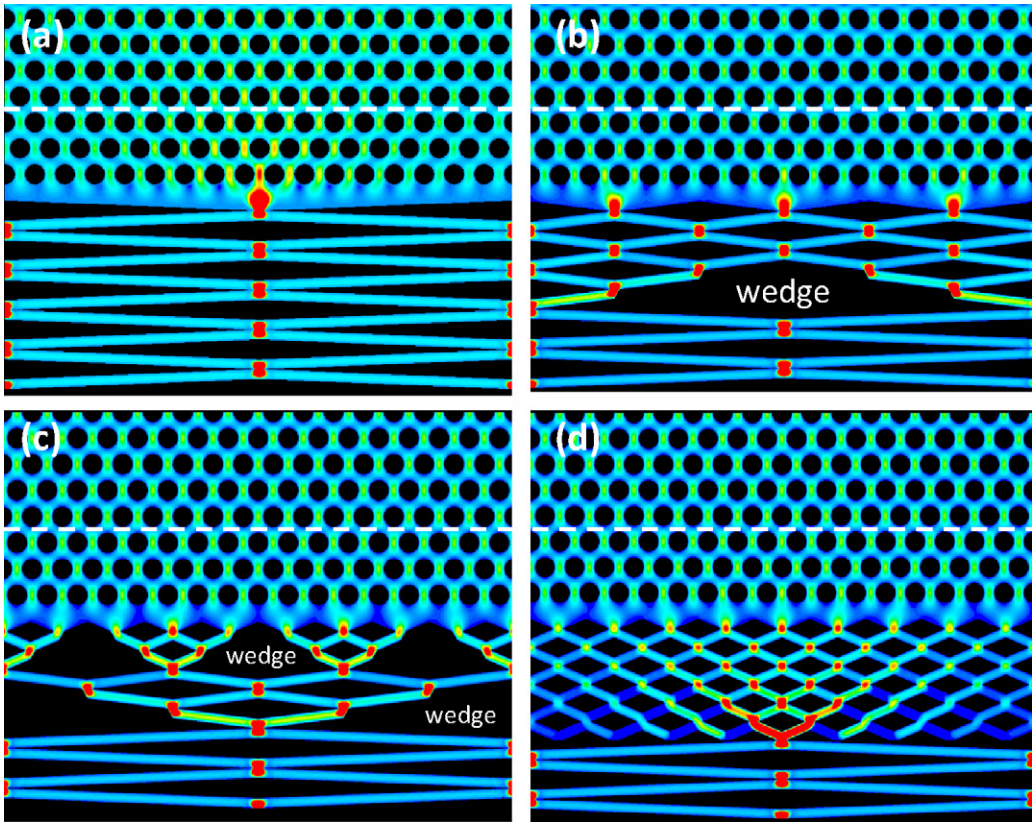

Fig. 10. Different mixed size distributors distributor considered to solve exit-point problem, showing (a) a single size distributor (AR = 25), (b) a two size distributor (AR = 25; AR = 8) with large "distributor wedges", (c) a three size distributor (AR = 25; AR = 8, AR = 2.33) with large "distributor wedges", and (d) a two size distributor (AR = 25; AR = 2.33) without "distributor wedges". ($\ell_p = 5\ \mu m$, $\delta_p = 2.5\ \mu m$, inlet velocity = 0.1 m/s, $D_{mol} = 10^{-9}$ m^2/s, transversal domain size = 63.75 μm ∼ AR 25).

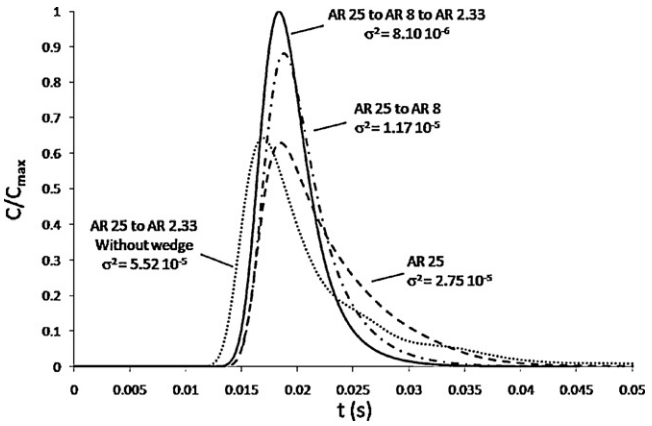

Fig. 11. Shape of bands eluting from distributors represented in Fig. 15 and corresponding variance values (calculated using Eqs. (6) and (7)).

ing a sample plug at the inlet of the flow domain and monitoring its peak width after the third pillar of the cylindrical pillar bed (monitor lines are indicated by white dashed lines in Fig. 10). The resulting band shapes are shown in Fig. 11. As the represented profiles have been obtained by averaging the species eluting from the distributor across the transversal direction of the flow domains represented in Fig. 10, these bands combine the local warp and the local axial dispersion (not the global warp, but this can anyhow be eliminated as much as desired by making the first part of the distributor, i.e., the part with the AR = 25 diamonds, sufficiently long).

As can be seen from Fig. 11, the three mixed size distributors perform significantly better than the single size distributor. Compared to the pure single size AR 25 distributor, the variance of the eluting peaks can be reduced by some 70% by arranging three different pillar sizes in three subsequent zones.

Crucial to the performance of the mixed size distributors is the introduction of so-called distributor wedges (See Fig. 10b and c). These wedges help preventing the formation of a stagnant zone in the wakes of the diamonds making up the last row of high AR pillars. The stagnant zone that would form without them can be clearly observed in Fig. 10d (the blue zones left and right, directly after the transition). The influence of these zones on band broadening upon transition is detrimental, the corresponding profile in Fig. 11 shows its performance is even worse than the single size AR 25 distributor.

4. Conclusions

Designing a flow distributor with uniform cross-section (divergence angle $\alpha = 180^\circ$), it can be advantageous to leave a small open zone just in front of the actual distributor bed. This region provides a direct transversal flow path for the fluid entering the channel and thus helps achieving the high transversal over axial permeability ratio that is needed to obtain a well-performing flow distributor. The axial width of this zone however needs to be optimised carefully. When the axial width of the zone is too small, the flow resistance in the transversal direction is too high and only a small fraction of the entering fluid is diverted into this direct transversal flow path. On the other hand, when the axial width of the pre-distributor zone is too large, a considerable axial dispersion will be generated because of the parabolic flow that will establish in the open zone. In addition, major parts of the open zone will be poorly permeated and will therefore act as a dead zone. For the presently considered geometry, the optimal axial width of the open pre-distributor zone was about 5 μm, i.e., about twice the width of the through pores in the actual distributor.

A second important design parameter is the aspect ratio (AR) of the distributor elements (pillars) making up the actual distributor (assuming the axial dimensions of the pillars are set by the machining limitations). Both from the perspective of maximizing the uniformity of the velocity profile as from the perspective of minimizing the axial dispersion, the AR of the pillars should be made as high as possible (a high AR implies here that the pillars are much more extended in the transversal than in the axial direction). The latter is less obvious, as one could have anticipated that the local axial dispersion would strongly increase when the AR of the pillars is increased. But this turns out not to be the case, especially also not because the use of higher AR pillars allows to significantly shorten the length of the distributor. Calculations furthermore showed that the additional flow resistance that would be introduced by applying distributor elements with an AR as high as 25 can still easily be tolerated.

High AR pillars however have the inherent drawback that they only redistribute the flow over a small number of discrete exit points (entry points in the case of an outlet distributor). As a consequence, a new flow distribution problem is created at each exit point. The obvious solution for this problem is to construct flow distributors that first consist of a zone filled with several rows of distributor elements (pillars) with a very high AR to produce a sufficiently uniform velocity profile, followed by one or more zones consisting of pillars with a smaller AR to increase the number of exit points and bring it sufficiently close to the number of parallel through pores in the actual separation bed. The best possible way to design such a mixed size distributor is by providing so-called "distributor wedges", that prevent the formation of poorly permeated zones in the wake of the pillars of the last row of high AR pillars. With such a design, the variance of the eluting bands can be reduced to only 30% of the variance of the bands eluting from a single size distributor.

Nomenclature

A	cross-section of column
AR	aspect ratio
d_{trans}	transversal domain size of distributor pillar grid (m)
d_{ax}	axial domain size of distributor pillar grid (m)
D_{mol}	molecular diffusion coefficient (m^2/s)
D_{ax}	axial dispersion coefficient (m^2/s)
D_{trans}	transversal dispersion coefficient (m^2/s)
ΔP	pressure drop (Pa)
δ	gap width before distributor (m)
δ_p	minimal inter pillar distance (m)
ε	porosity
F	volumetric flow rate (m^3/s)
FQ	frit quality
H	theoretical plate height (m)
h	dimensionless theoretical plate height
K_v	bed permeability (m^2)
ℓ	distributor length (m)
L	column length (m)
ℓ_p	axial pillar length (m)
μ	dynamic viscosity (Pa s)
M_0, M_1, M_2	zeroth, first and second moment
ν	Peclet number, dimensionless velocity
σ^2	variance (m^2)
t	time (s)
u_{mean}	mean axial velocity (m/s)
u_{centre}	mean axial velocity in centre of column (m/s)
u_{outer}	mean axial velocity in the pores nearest to the side wall (m/s)
w_p	transversal pillar width (m)
w	column width (m)

Acknowledgements

J. Vangelooven is supported through a specialisation grant from the Instituut voor Wetenschap en Technologie (IWT) from the Flanders region.

References

[1] B. He, F. Regnier, J. Pharm. Biomed. Anal. 17 (1998) 925.
[2] A. Fonverne, et al., Sens. Actuators B 129 (2008) 510.
[3] O. Gustafsson, et al., J. Micromech. Microeng. 18 (2008) 055021.
[4] H. Eghbali, S. Matthijs, V. Verdoold, H. Gardeniers, G. Desmet, J. Chromatogr. A 1216 (2009) 8603.
[5] M. De Pra, W. De Malsche, G. Desmet, P. Schoenmakers, W. Kok, J. Sep. Sci. 30 (10) (2007) 1453.
[6] J. Giddings, M. Schure, M. Myers, G. Velez, Anal. Chem. 56 (12) (1984) 2099.
[7] P. Williams, S. Giddings, J. Giddings, Anal. Chem. 58 (1986) 2397.
[8] H. Sant, J. Kim, B. Gale, Anal. Chem. 78 (23) (2006) 7978.
[9] J. Vangelooven, W. De Malsche, J. Op De Beeck, H. Gardeniers, G. Desmet, Lab Chip 10 (3) (2010) 349.
[10] Y. Wu, C. Ching, Chromatographia 57 (2003) 329.
[11] H. Boysen, G. Wozny, G. Guiochon, Chem. Eng. Technol. 27 (4) (2004) 369.
[12] S. Griffiths, R. Nilson, Anal. Chem. 73 (2001) 272.
[13] R. Qiao, N. Aluru, Sens. Actuators A 104 (2003) 268.
[14] J. Molho, et al., Anal. Chem. 73 (2001) 1350.
[15] C. Tsai, R. Yang, C. Tai, L. Fu, Electrophoresis 26 (2005) 674.
[16] K. Gebauer, X. Luo, N. Barton, A. Stokes, J. Chromatogr. A 1006 (2003) 45.
[17] Q. Yuan, A. Rosenfeld, T. Root, D. Klingenberg, E. Lightfoot, J. Chromatogr. A 831 (1999) 149.
[18] F. Lode, A. Rosenfeld, Q. Yuan, T. Root, E. Lightfoot, J. Chromatogr. A 796 (1998) 3.
[19] M. Lisso, G. Wozny, W. Arlt, A. Beste, Chem. Ing. Tech. 72 (2000) 494.
[20] J. De Smet, et al., J. Chromatogr. A 1073 (2005) 43.
[21] A. Neue, U. Berdichevsky, J. Chromatogr. A 535 (1990) 189.
[22] R. Aris, Proc. R. Soc., Lond. A 252 (1959) 538.